



Performance investigation of advanced adsorption desalination cycle with condenser–evaporator heat recovery scheme

Kyaw Thu^a, Young-Deuk Kim^a, Aung Myat^b, Anutosh Chakraborty^c, Kim Choon Ng^{b,*}

^aWater Desalination and Reuse Center, 4700 King Abdullah University of Science and Technology, Thuwal 23955-6900, Kingdom of Saudi Arabia

^bDepartment of Mechanical Engineering, National University of Singapore, 10 Kent Ridge Crescent, Singapore 117576, Singapore

Tel. +65 6516 2214; email: mpengkc@nus.edu.sg

^cSchool of Mechanical and Aerospace Engineering, Nanyang Technological University, 50 Nanyang Avenue, Singapore 639798, Singapore

Received 2 March 2012; Accepted 10 May 2012

ABSTRACT

Energy or heat recovery schemes are keys for the performance improvement of any heat-activated cycles such as the absorption and adsorption cycles. We present two innovative heat recovery schemes between the condensing and evaporating units of an adsorption desalination (AD) cycle. By recovering the latent heat of condenser and dumping it into the evaporative process of the evaporator, it elevates the evaporating temperature and hence the adsorption pressure seen by the adsorbent. From isotherms, this has an effect of increasing the vapour uptake. In the proposed configurations, one approach is simply to have a run-about water circuit between the condenser and the evaporator and a pump is used to achieve the water circulation. This run-around circuit is a practical method for retrofitting purposes. The second method is targeted towards a new AD cycle where an encapsulated condenser–evaporator unit is employed. The heat transfer between the condensing and evaporative vapour is almost immediate and the processes occur in a fully integrated vessel, thereby minimizing the heat transfer resistances of heat exchangers.

Keywords: Desalination; Adsorption; Heat recovery; Solar energy

1. Introduction

Potable water is a basic and essential resource that permeates all human activities such as agriculture, industrial and domestic sectors [1]. With increasing

economic development and population, freshwater demand of the world is expected to grow 2% annually to 6,900 billion or Gm³ in 2030 from today's 4,500 Gm³. The sustainable water supply from the earth's natural

*Corresponding author.

Table 1
Desalination method and capacity

Desalination method	Total capacity ($\times 10^6 \text{ m}^3/\text{day}$)	% by capacity
RO	37	59
MSF	17	27
MED	6	9
ED	2	4
Others	1	1
Total	63	100

water cycle is presently at $4,200 \text{ Gm}^3$ [2–8]. Water scarcity is one of the most critical problems faced by the governments in the countries around semi-arid and desert regions, as well as the land scarce and highly populated countries. The shortfall between demand and supply of water in such countries could be met by energy-intensive desalination of the seawater, brackish and recycled water. Presently, the commercially proven desalination methods are the multi-stage flash (MSF), the multi-effect distillation (MED), reverse osmosis (RO) and others such as vapour compression, electro-dialysis (ED), etc., as shown in Table 1 [9].

Two dominant desalination technologies are used worldwide and they are the MSF and the RO. In terms of the shares of the total online capacity of 60 million cubic meters, the RO technology represents 59% with more than 14,000 plants of assorted capacities, whilst the MSF has a 27% share [10]. The MSF and the MED plants are widely practised in the Middle East and North Africa region, and each plant has a water production capacity up to $100,000 \text{ m}^3$ per day. The reasons for having such thermally activated plants are that: (i) the high salinity of seawater found in the region (>45 ppt as opposed to 32–35 ppt in other parts of the world) and (ii) the frequent occurrence of bacteria blooms (algae/red tides) in the seawater of the Gulf region. The evaporative processes in the MSFs and MEDs are less affected by the above mentioned factors. Another key reason pertains to the availability of cheaper fossil fuels that favours the implementation of cogeneration in the thermal power plants: The integration of thermal desalination methods as a bottoming cycle to extract low pressure steam from the gas or steam-turbine power plants [11,12]. Such a cogeneration concept is widely implemented, leading to high-energy utilization of the primary fossil fuels for electricity and water production. For a given top-brine temperature from the exhaust of low pressure turbines, the MSF and MED designs maximize the recovery of latent heat of condensation/evapora-

tion processes at each successive stages, leading to a high Gain to Output Ratio [13] for the MSFs and the MEDs.

The membrane-based RO desalination systems utilize a pressure differential to overcome the osmotic pressure of saline solution through a semi-permeable membrane where suitably organized pore layers on the membrane permit the smaller water molecules to pass through. Osmotic pressure varies with the salinity and it is about 10–15 bar for brackish water systems and 50–80 bar for seawater systems [14,15]. The required pressure to push less concentrated permeate through membrane is generated by electrically driven pumps. Over the recent years, improved membrane technology and better energy recovery systems have yielded RO systems to have specific energy consumption between 2.5 and $4.3 \text{ kWh}/\text{m}^3$ [16,17]. Despite the low specific energy consumption, the drawbacks of RO systems are the product water quality in terms of residuals of boron, chlorides, bromides as well as the high maintenance of mechanical equipment and short membrane lifespan [18].

All desalination (other than the natural water cycle) technologies require either electricity or thermal heat, which requires the burning of primary energy fossil fuels. The exhaust of the power plants emits greenhouse gases (CO_2 , CH_4 and N_2O) that have the associated environmental issues such as global warming, etc. With increasing demand for freshwater, there is motivation for engineers and scientists to develop novel desalination technologies that are both energy efficient and yet environment-friendly. To this end, however, new emerging methods for desalination have been developed and tested, such as the membrane distillation, forward osmosis and AD. The key criteria for evaluating such desalination methods are: (i) reducing the specific energy consumption of desalting process to a level close to the thermodynamic limit of $0.8 \text{ kWh}/\text{m}^3$, (ii) minimizing chemical usage for the pre- and post-treatment of water and (iii) achieving lower targets for both carbon dioxide and brine discharge.

This paper presents the development of an advanced adsorption desalination (AD) cycle, one type of thermal desalination [19,20], which utilizes a low-temperature waste heat for the regeneration of the adsorbents, namely silica gel during every half cycle of the batch operation. As most of the major components used in an AD plant are stationary, and only waste heat is consumed, the specific energy needed to the AD cycle is only $1.38 \text{ kWh}/\text{m}^3$, and this is almost twice that of the thermodynamic limit for desalination. In this paper, we present an enhanced AD cycle with novel heat recovery schemes where the

latent heat of condensation of vapour is extracted and dumped into the evaporation process of saline water: such a design achieves a pressurization effect on the adsorbent and this increases the vapour uptake during the adsorption process.

We propose two possible configurations for the heat recovery process: in the first configuration, a run-around water circuit is used between the evaporator and condenser units and a suitable flow rate of water is pumped through the evaporator and condenser. Another approach is to encapsulate the evaporator and condenser as an integrated unit and this saves the pumping power needed to move the transporting coolant. The former approach is experimented in a pilot plant in the laboratory of the National University of Singapore whilst the performance of an integrated evaporator–condenser configuration is based on process simulation. The predicted and experimental results of the advanced AD cycles are analysed in terms of the specific daily water production (SDWP) and the performance ratio (PR).

2. Description of the advanced AD cycle

In AD cycles, desalination of saline water is achieved by adsorption-triggered-evaporation and desorption-aided-condensation processes and the plant comprises three major components, namely (i) the adsorber/desorber bed, (ii) the evaporator and (iii) the condenser. Evaporative boiling of the saline solution is achieved by the high water vapour affinity of adsorbent, namely, silica gel ($\text{SiO}_2 \cdot n\text{H}_2\text{O}$). Such adsorbents are hydrophilic with surface area in excess of $800\text{ m}^2/\text{g}$ and they are packed around the outer tube surfaces of heat exchangers, housed with vacuumated reactors or beds. The processes are arranged to operate in a batch-type cycle [21,22]. In an adsorption process, unsaturated silica gel is exposed to the evaporator filled with seawater. Owing to the high affinity for water vapour, immediate vapour uptake occurs, triggering an evaporative process that achieves the desalting phenomenon where dissolved salts remain in the solution. The drawn vapour is attached to the pores of the silica gel and remains captured by the van der Waals forces—a process known as physical sorption. The molecular kinetic energy is trapped and thus, the adsorption process is an exothermic and this rapid enhanced sorption is facilitated by cooling the adsorbent. Concomitantly, the previously saturated adsorbent is now fed with a heat source from circulating hot water in the heat exchanger. The rise in the adsorbent temperature from heating increases the

vibrational energy of captured vapour molecules within the pores, and until a critical level is reached, the water vapour leaves the pore surfaces to become free vapour molecules. This process is termed as the desorption process and desorption continues until the preset half-cycle time is reached. The desorbed vapour travels to cooler tube surfaces within a condenser unit and condenses to give pure distillate as potable water.

In an advanced AD cycle, the heat recovery from the condensation to the evaporation of the saline water is introduced to enhance the water production rate. This type of heat recovery can be implemented using two configurations: (1) with a heat recovery circuit running across the evaporator and the condenser and (2) the encapsulated evaporator–condenser device. Fig. 1 shows the schematic diagrams of an advanced AD cycle with the evaporator–condenser heat recovery scheme. Fig. 1(a) gives the schematics of Configuration_1 with heat recovery circuit between the evaporator and the condenser whilst Fig. 1(b) shows the schematics of Configuration_2 with an encapsulated evaporator–condenser device. The first configuration is suitable for existing AD cycles that can be readily configured with a slight modification to the piping arrangement. It provides the operation flexibility to switch the operation modes between dual-effect (cooling and desalination) and single purpose (desalination) modes whereas the latter configuration is optimized for desalination.

The latter cycle employs an enclosed evaporator–condenser device where it can be either a shell and tube-type or plate-type heat exchanger. Here a shell and tube type with horizontal tube heat exchanger is considered for the evaporation of saline water in the shell side and the condensation of the water vapour in the tube side. It is noted that both the condenser and the evaporator heat transfer water circuits used in the conventional AD cycle are eliminated and hence, a significant saving in the pumping cost is realized in advanced AD cycle. Condensation heat is transferred directly across the walls of the condenser tubes to the evaporator. This arrangement reduces the heat transfer resistances, leading to an improvement in the evaporation rates of water vapour from the seawater solution.

The advantage of the advanced AD cycle with this kind of heat recovery is the pressurization of the adsorption environment through higher vapour pressure in the evaporator, and this has a direct effect of increasing the vapour uptake by the silica gel during the adsorption process. Thus, the advantages of the advanced AD cycle (with condenser–evaporator heat recovery) are summarized as follows:

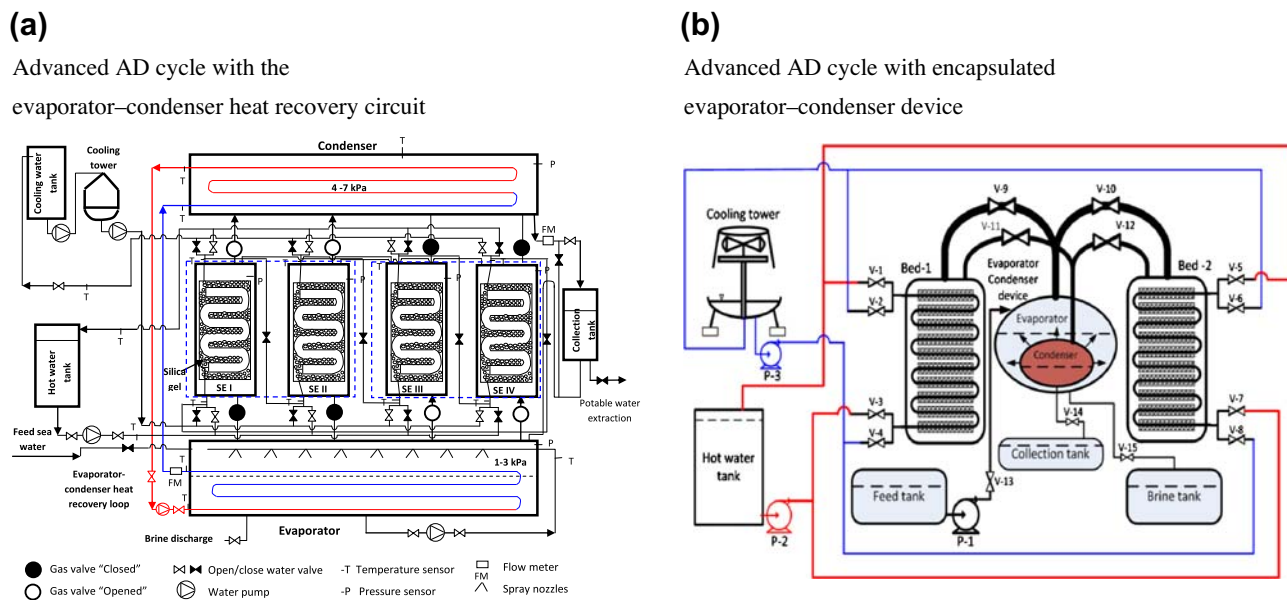


Fig. 1. Schematic diagrams of advanced AD cycle.

- (1) a reduction in the parasitic electrical power owing to the elimination of pumps for the chilled and cooling water circuits,
- (2) an improvement in the adsorption capacity of silica gel due to the pressurization effect,
- (3) a lowering of the effective condensation temperature in condenser and this tends to desorb more vapour during the desorption process, and
- (4) the ability to operate low temperature of heat source at 50°C or higher.

3. Mathematical modelling

A mathematical model on an advanced AD cycle that employs the internal heat recovery process was developed to access the performance of the cycle. Iso-

therm and kinetics properties of the silica gel–water pair are employed to predict the uptake of the water vapour by the silica gel at specific temperature and pressure conditions. Type A⁺⁺ silica gel was used as the adsorbent and Table 2 shows the physical properties of Type A⁺⁺ silica gel.

A complete numerical modelling of the advanced AD cycles considering all the components involved are listed in Table 3. These model equations cover both configurations of heat recovery.

Here, $M_{s,Evap}$ is the amount of seawater in the evaporator, $\dot{m}_{s,in}$ is the rate of feed seawater, $\dot{m}_{d,Cond}$ is the mass of potable water extracted from the condenser, and \dot{m}_{Brine} is the mass of concentrated brine rejected from the evaporator. The feed seawater is intermittently pumped into the evaporator depending on the amount and level of seawater, whilst brine is discharged once the concentration in the evaporator reaches the predetermined limit. In the concentration balance equation, $X_{s,in}$ and $X_{s,Evap}$ are the concentration of the feed and seawater in the evaporator X_D is the concentration of the vapour, whilst the values θ , γ , and n are the flags in the equations during operation and switching processes which are listed in Table 4.

The evaporation of seawater is attributed to the uptake of the water vapour by the adsorbent and the energy recovered from the condensation is used to maintain the evaporation process at a certain temperature level.

The first term in the right-hand side of the evaporator energy balance equation represents the sensible heat by the supplied feed seawater, the second term

Table 2
Physical properties of Type A⁺⁺ silica gel

Property	Value
Pore size (nm)	0.8–7.5
Porous volume (cm ³ g ⁻¹)	0.476
Surface area (m ² g ⁻¹)	863.6
Average pore diameter (nm)	2.2
Apparent density (kg m ⁻³)	700
pH	4.0
Specific heat capacity (kJ kg ⁻¹ k ⁻¹)	0.921
Thermal conductivity (W m ⁻¹ k ⁻¹)	0.198

Table 3
A summary of the numerical modelling of advanced AD cycles

	Configuration_1	Configuration_2
Balance equation		
Adsorption isotherm	$q^* = q_0 \exp[-(\frac{RT}{P}) \ln(\frac{P}{P_0})^n]$	
Adsorption kinetics	$\frac{dq}{dt} = \frac{15D_{a,0} \exp(-\frac{E_a}{RT})}{R^2} (q^* - q)$	
Isosteric heat of adsorption	$Q_{st} = h_{fg} + E \{ -\ln(\frac{P}{P_0}) \}^{1/n} + T v_g (\frac{\partial P}{\partial T})_g$	
c_p of adsorbed phase	$c_{p,a} = c_{p,g} + \{ \frac{1}{T} - \frac{1}{v_g} (\frac{\partial v_g}{\partial T})_p \} Q_{st} - \frac{\partial Q_{st}}{\partial T} P$	
Concentration balance	$M_{s,Evap} \frac{dX_{s,Evap}}{dt} = \theta X_{s,in} \dot{m}_{s,in} - \gamma X_{s,Evap} \dot{m}_{Brine} - n X_D \frac{dX_{s,ads}}{dt} M_{sg}$	$[M_{s,Evap} c_{p,s} (T_{Evap}, X_{s,Evap}) + M_{HX,Evap} c_{p,HX}] \frac{dT_{Evap}}{dt} = \theta h_f (T_{Evap}, X_{s,Evap}) \dot{m}_{s,in} - n h_{fg} (T_{Evap}) \frac{dX_{s,ads}}{dt} M_{sg} + U_{EC} A (T_{Cond} - T_{Evap}) - \gamma h_f (T_{Evap}, X_{s,Evap}) \dot{m}_{Brine}$
Evaporator energy balance	$[c_{p,s} (T_{evap}) M_{s,evap} + M_{HX,Evap} c_{p,HX}] \frac{dT_{evap}}{dt} = \theta h_f (T_{evap}) \dot{m}_{s,in} - n h_{fg} (T_{evap}) M_{sg} \frac{dX_{s,ads}}{dt} + \dot{m}_{evap} c_{p,evap} (T_{chilled,in} - T_{chilled,out}) - \gamma h_f (T_{Evap}, X_{s,Evap}) \dot{m}_{Brine}$	$[M_{Cond} c_p (T_{Cond}) + M_{HX,Cond} c_{p,HX}] \frac{dT_{Cond}}{dt} = -h_f (T_{Cond}) \frac{dM_d}{dt} + U_{Overall} A (T_{Cond} - T_{Evap})$
Condenser energy balance	$[c_p (T_{cond}) M_{cond} + M_{HX,Cond} c_{p,HX}] \frac{dT_{cond}}{dt} = -h_f (T_{cond}) \frac{dM_d}{dt} + h_{fg} (T_{cond}) M_{sg} \frac{dX_{s,ads}}{dt} + \dot{m}_{cond} c_{p,cond} (T_{cond,in} - T_{cond,out})$	$(m c_p)_{ss} \frac{dT_{w2}}{dt} = h_{Cond} A_{Cond} (T_{Cond} - T_{w2}) - \frac{2\pi k L}{\ln \frac{r_2}{r_1}} (T_{w2} - T_{w1})$
Condenser wall temperature	-	
Evaporator-side wall temperature	-	$(m c_p)_{ss} \frac{dT_{w1}}{dt} = h_{Evap} A_{Evap} (T_{w1} - T_{Evap}) + \frac{2\pi k L}{\ln \frac{r_2}{r_1}} (T_{w2} - T_{w1})$
U of evaporator-condenser device	-	$U_{Overall} = (\frac{1}{h_{Cond}} + \frac{r_2 \ln \frac{r_2}{r_1}}{k} + \frac{r_2 - 1}{r_1 h_{Evap}})^{-1}$
h for evaporation	Experimental data	$T_w - T = (\frac{c_{p,eff} P_{eff}}{C_{p,f}}) \left[\frac{q_{evap}}{h_f h_{fg} \sqrt{\delta^{(n-1)g}}} \right]^n \times \left(\frac{P}{P_{atm}} \right)^m \left(\frac{A_{evap,ads}}{A_{base}} \right)^z$
h for condensation	Experimental data	$h = F \left[\frac{q_{ads,des} (\rho_1 - \rho_2) h_{fg} + \frac{3}{2} c_{p,l} (T - T_w) \right]^{0.25}}{D_{eff} (T - T_w)}$
Adsorber	$(M_{sg} c_{p,sg} + M_{HX,Ads} c_{p,HX} + M_{abe} c_{p,a}) \frac{dT_{ads,des}}{dt} = \pm Q_{st} (T_{ads,des}, P_{evap/cond}) n \times M_{sg} \frac{dX_{s,ads}}{dt} \pm \dot{m}_{cw/hw} c_{p,cw/hw} (T_{ads,des}) (T_{cw/hw,in} - T_{cw/hw,out})$	$[M_{sg} c_{p,sg} + M_{HX} c_{p,HX} + M_{abe} c_{p,a}] \frac{dT_{ads,des}}{dt} = \pm \dot{m}_{cw/hw, in} c_p (T_{cw/hw, in} - T_{cw/hw, out})$
Outlet water temperature	$T_{out} = T_0 + (T_{in} - T_0) \exp(\frac{-UA}{\dot{m}_{c_p}(T_0)})$	
Adsorber heat	$Q_{ads} = \dot{m}_{cw} c_{p,cw} (T_{cw,out} - T_{cw,in})$	
Desorber heat	$Q_{ads} = \dot{m}_{cw} c_{p,cw} (T_{cw,out} - T_{cw,in})$	
Evaporator heat	$Q_{Evap} = \dot{m}_{Evap} c_{p,Evap} (T_{Evap}) (T_{chilled,in} - T_{chilled,out})$	
Condenser heat	$Q_{cond} = \dot{m}_{cond} c_{p,cw} (T_{cond}) (T_{cond,out} - T_{cond,in})$	
SDWP	$SDWP = \int_0^{t_{cycle}} \frac{Q_{cond, \tau}}{h_{fg}(T_{Cond})} M_{sg} d\tau$	
PR	$PR = \frac{1}{t_{cycle}} \int_0^{t_{cycle}} \frac{\dot{m}_{d,Cond} h_{fg}(T_{Cond})}{Q_{des}} dt$	$Q_{Evap} = h_{Evap} A_{Evap} (T_{w1} - T_{Evap})$ $Q_{Cond} = h_{Cond} A_{Cond} (T_{Cond} - T_{w2})$

Table 4
Values of the indicators for changing the operation mode of the AD cycle

Mode	Parameter	Value
Operation	n	2
	θ	1 (charging sea water) 0 (otherwise)
	γ	1 (brine discharge) 0 (otherwise)
Switching	n	2
	θ	1 (charging sea water) 0 (otherwise)
	γ	1 (brine discharge) 0 (otherwise)

stands for the heat removal by the uptake of adsorbent, the third and fourth terms denote the energy supplied for the evaporation through heat recovery from the condensation process and the sensible heat removal by the brine discharge. The specific heat ($c_{p,s}$) and enthalpy (h_f) of seawater are calculated as functions of temperature, pressure and salinity.

As the evaporated seawater is associated onto the solid adsorbent by the flow of external cooling fluid during adsorption period, whilst the desorbed water vapour is dissociated from the solid adsorbent by the flow of heating fluid during desorption period, the heat energy is exchanged between the cooling/heating fluid and the adsorption/desorption bed. Here isosteric heat, Q_{st} , and the specific heat $c_{p,a}$ of the adsorbed phase are considered for better prediction [23].

Using the heat transfer Equation, the outlet temperature of water from each heat exchanger is estimated using the log mean temperature difference method.

The adsorption/desorption rate of water vapour by the silica gel is calculated from the knowledge of adsorption equilibrium and kinetics and is given by the conventional linear driving force equation, where D_{so} defines a pre-exponential factor of the efficient water diffusivity in the adsorbent, E_a represents the activation energy, R is the universal gas constant and R_p is the average radius of the adsorbent grains. Kinetic data were taken from [24,25]. The adsorption uptake at equilibrium condition is expressed as a function of pressure (P) and temperature (T). These experimentally measured data are fitted using the Dubinin–Astakhov equation.

After desorption, the desorbed water vapours are delivered to the condenser as latent heat and in advanced AD cycle, this energy is internally recovered for the evaporation process. In modelling, it is

assumed that the condenser tube bank surface is able to hold a certain maximum amount of condensate. Beyond this, the condensate would flow into the water collection tank via a U-tube.

For Configuration_2 i.e. the integrated evaporator–condenser design, the heat transfer coefficient of the boiling of the saline solution is predicted using the modified Rohsenow correlation for subatmospheric pressures [26] whilst Nusselt film condensation correlation is applied to calculate the heat transfer coefficient for condensation of the water vapour inside the condenser. The values of all the coefficients and the parameters used in the simulation are listed in Table 5.

For the desorption process, the energy required to desorb water vapour from the silica gels, Q_{des} , is calculated using the inlet and outlet temperatures of the heat source supplied to the reactors. Concomitantly, the energy rejected to the cooling water during the adsorption process is estimated by the inlet and outlet temperatures of the cooling fluid that is supplied to the other reactor.

The performance of the AD cycle is given by SDWP and PR, defined here as the ratio of useful effects to the energy input to the cycle.

These sets of energy and mass balance equations are solved by Adams–Moulton’s method in the DIVPAG subroutine of the IMSL FORTRAN math library subroutines. A double-precision accuracy was applied and the tolerance was set to 1×10^{-12} . The code runs on the platform of FORTRAN PowerStation. As the AD cycle is operated in a batch manner, the connection or pointers for linking one subroutine to another have to be carefully directed so that the correct boundary conditions are maintained during the computation. The cyclic steady-state condition can be achieved in 4 to 5 cycles after the commencement of computation.

4. Results and discussion

The advanced AD cycle with internal heat recovery between the condenser and the evaporator is investigated at various operation conditions such as different cycle times, hot and cooling water temperatures, different hot and cooling water flow rates. Fig. 2 depicts the pictorial view of the advanced AD plant showing the condenser–evaporator heat recovery circuit.

The transient temperature profiles of the major components of the advanced AD cycle that incorporates the heat recovery scheme between the condenser and the evaporator are shown in Fig. 3. In this analysis, the hot water inlet temperature was maintained at 70°C whilst the cycle time (t_{cycle}) and the switching

Table 5
Values of the parameters used in the simulation program

Parameter	Value	Unit
q_0	0.592	kg/kg of silica gel
E	3.105	kJ mole ⁻¹
n	1.1	–
D_{so}	2.54×10^{-4}	m ² s ⁻¹
E_a (kJ/kg)	4.2×10^{-4}	kJ kg ⁻¹
R_p	0.4	mm
Hot water inlet temperature	50–85	°C
Cooling water inlet temperature	30	°C
Mass of silica gel per bed, M_{sg}	36	kg
Adsorber/desorber bed heat transfer area	41.7	m ²
Tube length	0.576	m
$M_{HX}c_{p,HX}$	184.1	kJ K ⁻¹
U_{ads}	250 [27]	W m ⁻² K ⁻¹
U_{des}	240 [27]	W m ⁻² K ⁻¹
<i>Configuration_1 (Evaporator–condenser heat recovery circuit)</i>		
U_{evap}	1,715.2	W m ⁻² K ⁻¹
U_{cond}	2,657.5	W m ⁻² K ⁻¹
A_{evap}	3.5	m ²
A_{cond}	5.08	m ²
Thermal mass of the evaporator including fins and support	25.44	kJ K ⁻¹
Mass of refrigerant in the evaporator	250	kg
Thermal mass of the condenser including fins and support	18.61	kJ K ⁻¹
Mass of condensate in the condenser	10	kg
<i>Configuration_2 (Integrated evaporator–condenser)</i>		
L_{tube}	2.0	m
Number of tubes (stainless steel)	60	–
r_1	7.1	mm
A_{wetted}	9.35	m ²
A_{base}	4.67	m ²
A_{Cond}	5.35	m ²
c_p	500	J kg ⁻¹ K ⁻¹
k	16.2	W m ⁻¹ K ⁻¹
<i>Operation conditions</i>		
t_{cycle}	300–600	s
$t_{switching}$	20	s

time ($t_{switching}$) are kept 600 s with 40 s, respectively. It is noted that the experimental temperature measurements are subjects to the time constant and accuracy of the sensors. As can be observed from Fig. 3, the simulated results of transient temperature agree well with those of the experimental data, thus the simulation is being validated by the experiment. The hysteresis found in the condenser temperature resulted from the location of the sensor that is placed near the desorber vapour pipe. Thus, it fails to capture the temperature drop by the cold front from the evaporator at the beginning of the cycle operation.

Fig. 4 gives the SDWP and the PR of the advanced AD cycle whilst operating at different hot water inlet temperatures. The experimental results show that the SDWP linearly increases with the hot water inlet temperature and is about 9.24 m³/tonne of silica gel per day at 70°C hot water inlet temperature, whilst the SDWP reaches 14.2 m³/tonne of silica gel per day at 85°C hot water inlet temperature. The increase in the SDWP with the increase in the hot water temperature is attributed to the better desorption–condensation process at higher regeneration temperatures resulting in the increase in SDWP. It should be noted that the

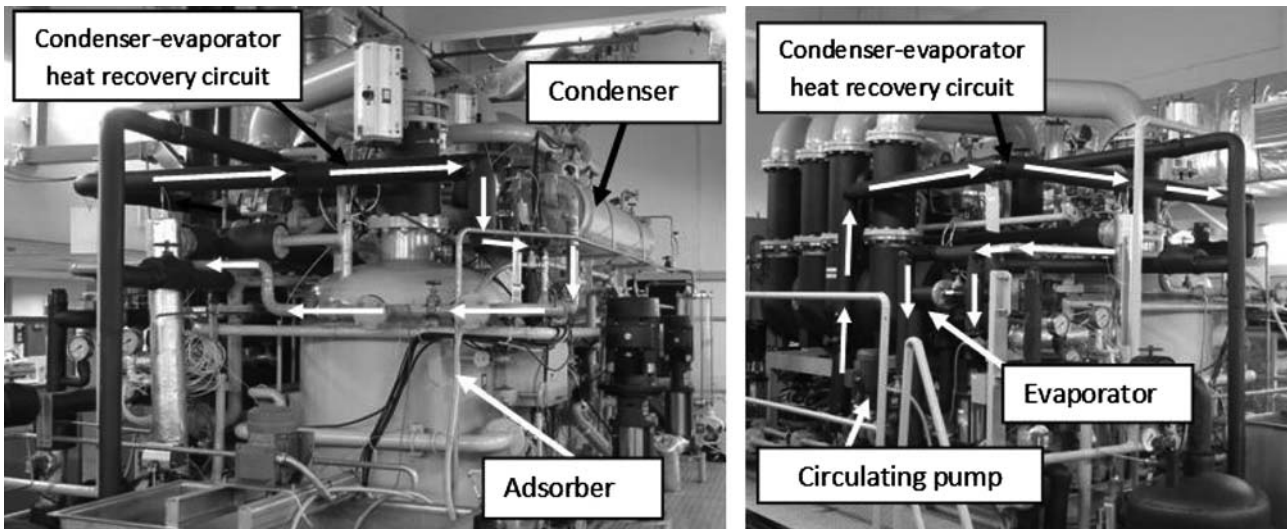


Fig. 2. Pictorial view of the AD cycle with the condenser–evaporator heat recovery circuit.

advanced AD cycle is capable of operating at a substantially low hot water inlet temperature, i.e. 50°C at which conventional AD cycle fails to operate and the produced SDWP is 5.2 m³ of potable water per tonne of silica gel per day.

The effect of the cooling water inlet temperature on the performance of the advanced AD cycle is shown in Fig. 5. The SDWP of the cycle for two sets of hot water inlet temperatures, i.e. 50 and 70°C, is presented whilst varying the temperature of the coolant from 26 to 32°C. A higher water production rate is

achieved at lower coolant temperatures whilst the production rate decreases as the coolant temperature is increased.

Fig. 6 shows the temperature–time history of the adsorber, desorber, evaporator and condenser of the advanced AD cycle with an evaporator–condenser device at the cyclic steady-state conditions. The temperatures of the heat source and cooling water are maintained at 85 and 30°C, respectively, whilst the half-cycle time is set at 300 s and the switching time 20 s. Owing to the integral evaporator–con-

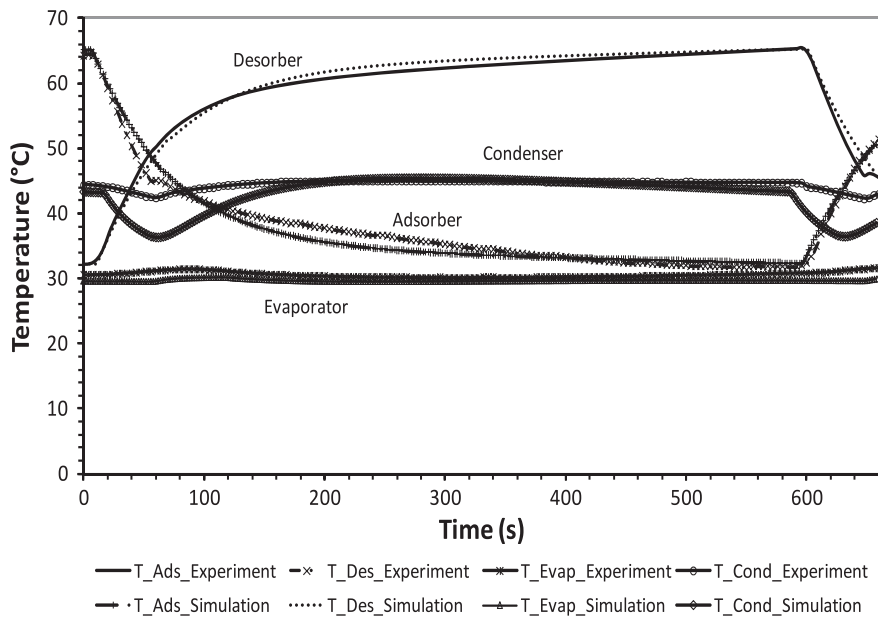


Fig. 3. The temperature profiles of the major components of the advanced AD cycle.

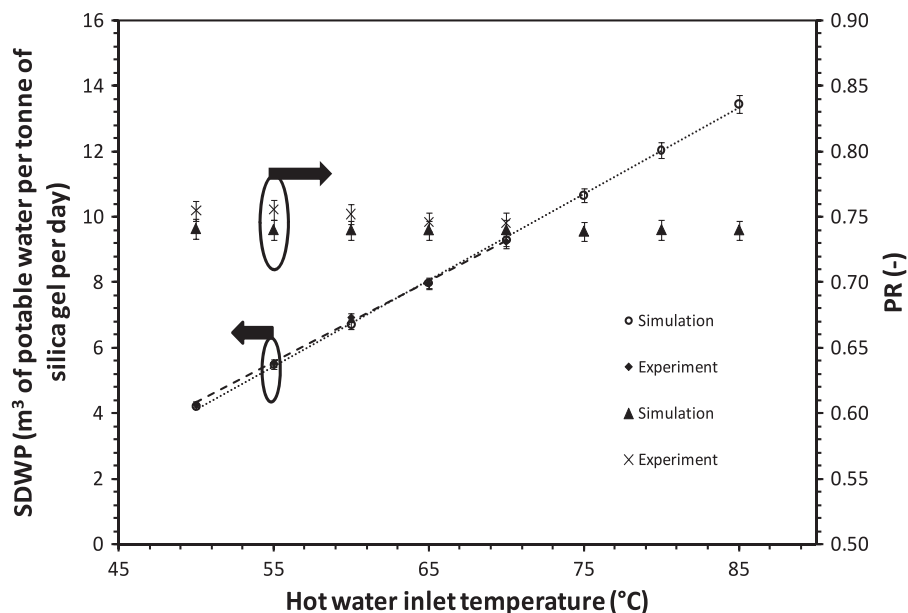


Fig. 4. The SDWP and PR of the advanced AD cycle with assorted hot water inlet temperatures ranging from 50°C to 70°C.

denser design, the pressurization effect on the adsorption–evaporation process is observed. This is achieved by bringing about an increase in the evaporation temperature, which is about 42°C through heat recovery from condensation. From the isotherm properties of silica gel–water pair, the higher adsorption pressure enhances the adsorption capacity by the adsorbent.

The improvement in the uptake of the adsorbent tends to a higher rejection of adsorption heat and subsequently the adsorption temperature. It is observed that the adsorber bed temperature is relatively high at

44°C whilst the condensation temperature is found to be about 48°C. The pressure profile of the cycle is given in Fig. 7 and it is noted that the operating pressure region of the advanced AD cycle is elevated to 7–12 kPa in contrast to the conventional cycle where the pressure ranges from 3 to 7 kPa. The performance of the evaporator–condenser device presented is given in Fig. 8 where the maximum temperature difference between the evaporator and the condenser wall is observed to be 1.3°C.

The performance of the evaporator–condenser device implemented in the advanced AD cycle is also analysed in terms of the overall heat transfer coefficient. The overall heat transfer coefficient of the evaporator–condenser unit is evaluated using the Modified Rohsenow correlation for subatmospheric conditions for evaporation and Nusselt film correlation for condensation. The thermal resistance imposed by the stainless steel tubes is also accounted for. The overall heat transfer coefficient (U) of the evaporator–condenser device is shown in Fig. 9.

The predicted data showed that the U value is higher at the beginning of every cycle and gradually lower with the cycle time. This is because the uptake and desorption amount by the silica gel is higher at the beginning of the cycle operation resulting in rapid boiling and condensation. Thus, the U value is higher at that period. The uptake amount gets diminished as the silica gel gets saturated as well as the desorption rate becomes slower as the cycle operation advances. However, during the switching period, the U value

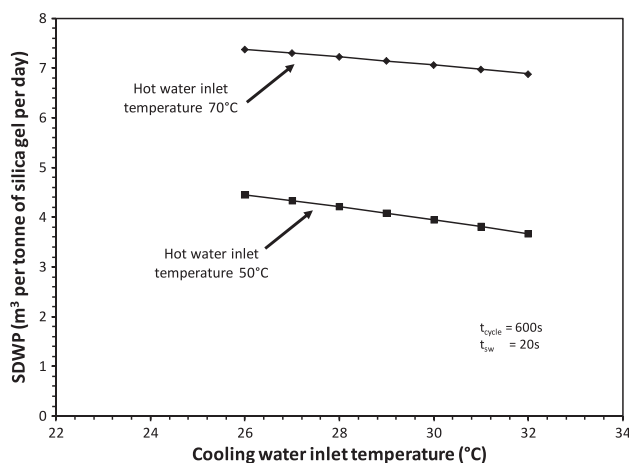


Fig. 5. The performance of the advanced AD cycle at different cooling water inlet temperatures.

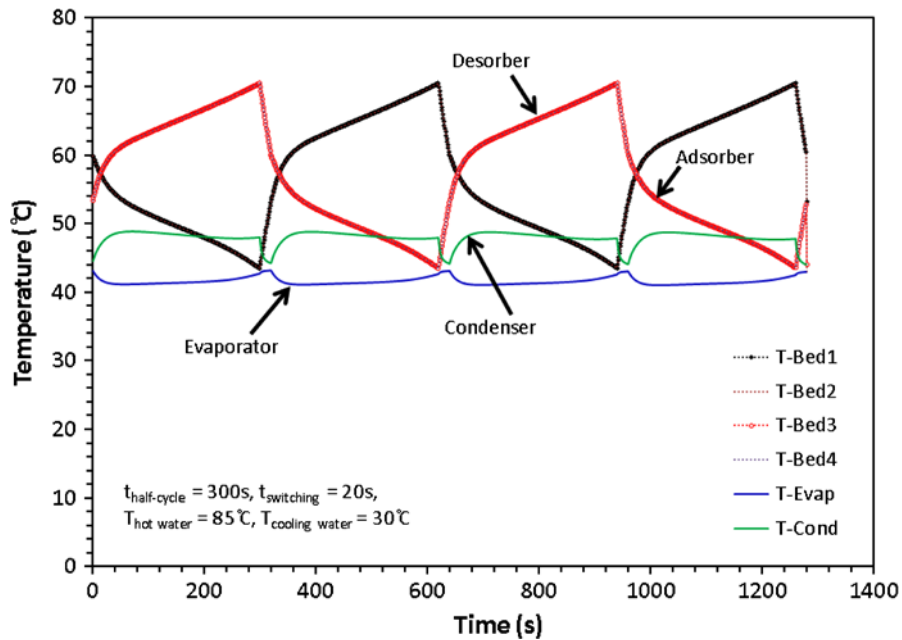


Fig. 6. Predicted temperature–time histories of the adsorber, desorber, evaporator, and condenser of the advanced AD cycle.

drops to a value less than $500 \text{ W m}^{-2} \text{ K}^{-1}$. This is because there are no adsorption and desorption phenomena in this period and the resultant small value of U is due to the exchange of heat between the thermal masses of the evaporator and the condenser. The average overall heat transfer coefficient (U_{Overall}) is found

to be about $2,300 \text{ W m}^{-2} \text{ K}^{-1}$, which is quite a good value across the vapour condensing in the condenser to the vapour leaving the saline solution falling over the surface of tubes of evaporator.

A parametric analysis on the advanced AD cycle was conducted to study the performance of the cycle

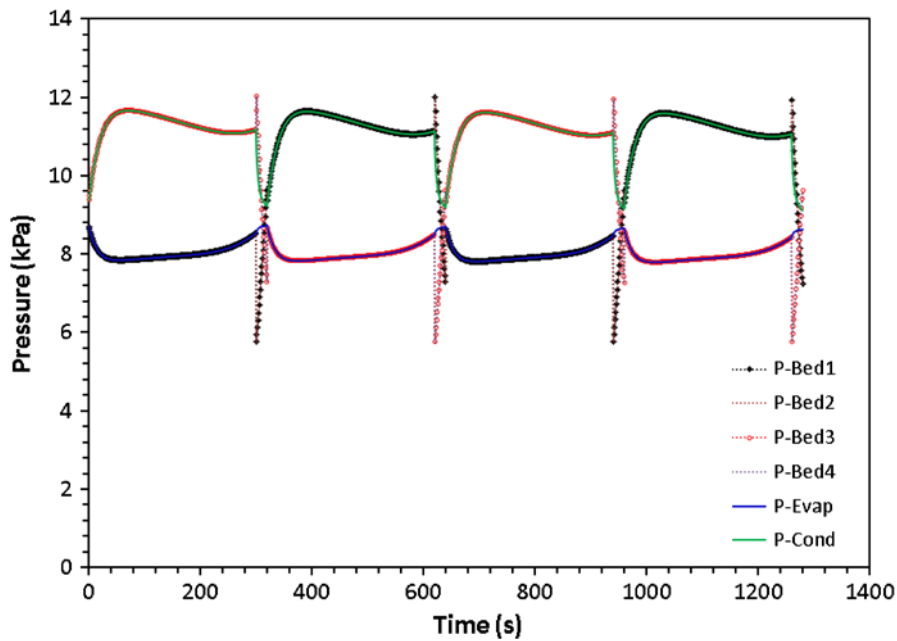


Fig. 7. The temporal pressure profiles of the advanced AD cycle.

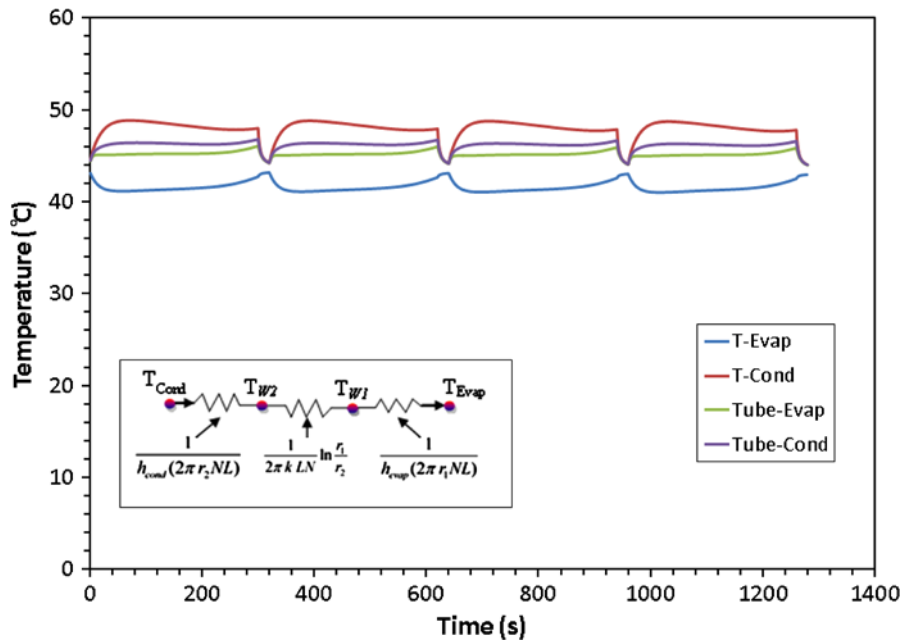


Fig. 8. Temperature profiles of the evaporator–condenser device in advanced AD cycle.

at various operating conditions such as different cycle times, different hot and cooling water inlet temperatures to the adsorber beds.

Fig. 10 represents the SDWP of the advanced AD cycle for assorted regeneration temperatures from 50 to 85°C. The results show that the water production

rate of the advanced cycle linearly varies with the hot water temperature. This is due to a better regeneration process for higher hot water temperatures.

The effect of cooling water temperature on the performance of the advanced AD cycle is also investigated. The temperature range between 25 and 35°C is

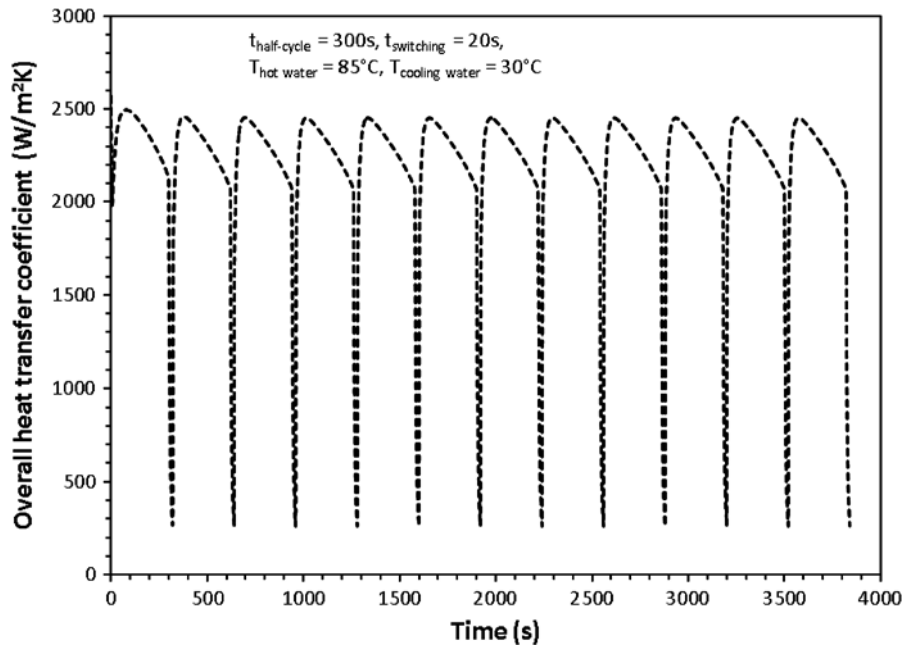


Fig. 9. Overall heat transfer coefficient of the evaporator–condenser device.

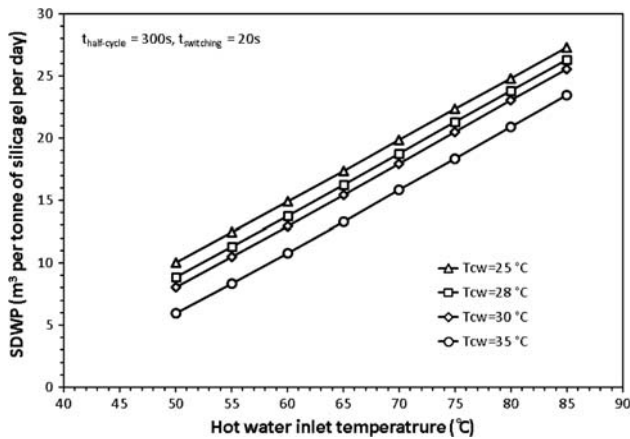


Fig. 10. The predicted SDWPs and overall heat transfer coefficients of the advanced AD cycle at assorted hot water inlet temperatures.

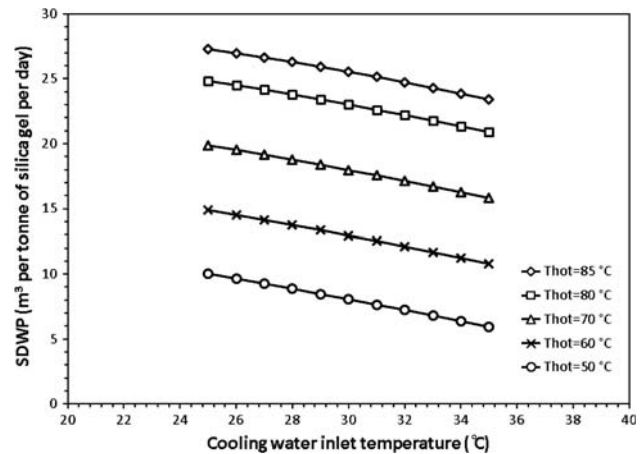


Fig. 11. The predicted potable water production of the advanced AD cycle for different cooling water inlet temperatures.

selected as this is a practical cooling water temperature range readily available using a conventional cooling tower. The effect of the cooling water temperature on the cycle is investigated at assorted hot water inlet temperatures between 50 and 85 °C. The performance of the cycle in terms of SDWP is presented in Fig. 11 in which the results show that the cycle performs more efficiently at a lower cooling water temperature giving a higher SDWP. As the cooling water temperature increases, the SDWP of the cycle becomes lower. This phenomenon can be attributed to the isotherm behaviour of the silica gel where the lower-temperature

adsorption environment promotes uptake capacity by the adsorbent.

A comparison on the water production rates by different adsorption cycles at normalized cycle times and same operating conditions ($T_{hot} = 85\text{ °C}$ and $T_{cw} = 30\text{ °C}$) is given in Fig. 12. A conventional AD cycle and an AD cycle with heat recovery between condenser and evaporator using an evaporator–condenser heat recovery circuit are selected for the comparison [20–30]. It is noted that experimental data for the aforementioned cycles are used here. The results show that the advanced AD cycle can produce potable water up to threefold of the

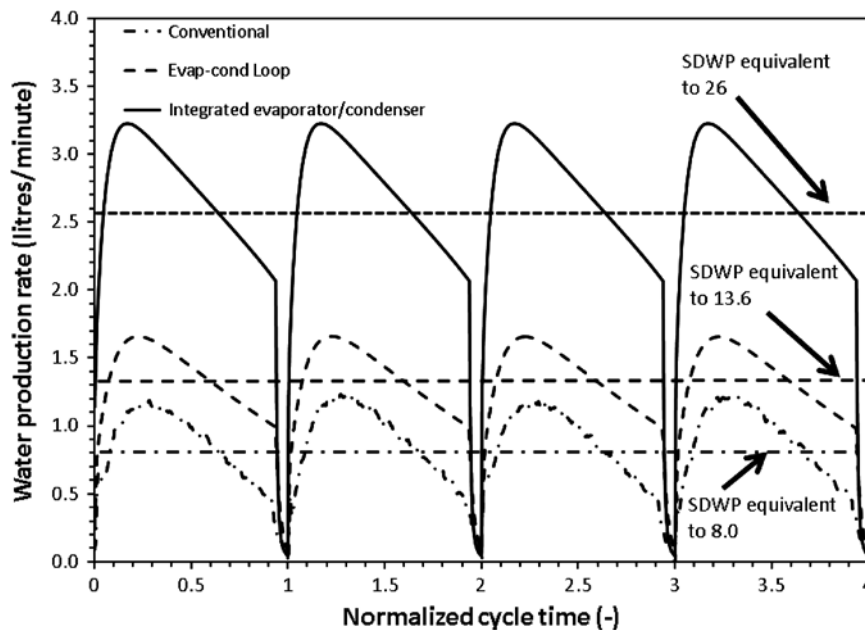


Fig. 12. Comparison on the water production rates by different AD cycles at typical operating conditions.

conventional cycle whilst it produces twice that of the AD cycle with an evaporator–condenser heat recovery circuit. Another significant advantage of the advanced cycle is that it can be operational at hot water inlet temperatures as low as 50°C whilst a conventional cycle is unable to do so at such low temperatures. This low-grade regeneration temperature is readily available from the solar thermal sources or waste heat from processes. The SDWP at 50°C hot water inlet temperature is found to be about 8.1 m³ per day that is comparable with that of the conventional cycle even at this low heat source temperature.

5. Conclusions

We have presented an advanced AD cycle for desalination where the internal latent heat between the evaporator and condenser units is recovered. This is equivalent to having a compressor to pressurize the adsorbent during adsorption, and thus making the adsorbent have a higher water vapour uptake. Two configurations have been described and they have been proven to be feasible and practical. Retrofitting using a run-around loop was readily implemented on an existing AD plant and an increase in the water production was measured. In the NUS's pilot plant, the run-around heat recovery procedure increases the SDWP to 9.24 m³/tonne-day, despite a low heat source inlet of 70°C. At an inlet hot water of 85°C, the water production of the retrofitted AD cycle attains a SWDP of 14.2 m³/tonne-day. On the other hand, the simulated results from an integrated condenser–evaporator design show higher yields, up to a threefold increase in SWDP: at 55°C hot water inlet to the AD cycle, a SWDP of 8.1 m³/tonne-day could be achieved whilst SWDP of 26 m³/tonne-day is attained at 85°C. Such increases are attributed to the higher heat transfer coefficient of the integrated design, typically around 2,300 W/m²K.

Symbols

σ	—	surface tension, N m ⁻¹
α	—	constant in modified Rohsenow correlation, —
ρ	—	density, kg m ⁻³
γ	—	flag which governs the mode of operation, —
θ	—	flag which governs the mode of operation, —
q''	—	heat flux, W m ⁻²
\dot{m}	—	mass flow rate, kg s ⁻¹
τ	—	number of cycles per day, —

μ	—	viscosity, kg m ⁻¹ s ⁻¹
A	—	area, m ²
COP	—	the coefficient of performance, —
c_p	—	specific heat capacity, J kg ⁻¹ K ⁻¹
C_{sf}	—	a constant of Rohsenow correlation, —
D_{so}	—	a kinetic constant for the silica gel water system, m ² s ⁻¹
E_a	—	activation energy of surface diffusion, kJ mol ⁻¹
g	—	gravitational acceleration, m s ⁻²
h_f	—	sensible heat, kJ kg ⁻¹
h_{fg}	—	latent heat, kJ kg ⁻¹
k	—	the thermal conductivity, W m ⁻¹ K ⁻¹
L	—	length, m
m	—	constant in modified Rohsenow correlation, —
M	—	mass, kg
n	—	number of beds/constant in modified Rohsenow correlation, —
P	—	pressure, Pa
P_0	—	reference pressure, Pa
PR	—	performance ratio, —
q	—	concentration, kg kg ⁻¹
Q	—	the total heat or energy, W or J
q^*	—	the equilibrium uptake, kg kg ⁻¹
q^o	—	the limiting uptake, kg kg ⁻¹
Q_{st}	—	isosteric heat of adsorption, kJ kg ⁻¹
r	—	radius, m
R	—	Universal gas constant, J K ⁻¹ mol ⁻¹
R_p	—	average radius of silica gel, m
SDWP	—	specific daily water production, m ³ /tonne-day ⁻¹
T	—	temperature, K
t	—	time, s
T_0	—	reference temperature, K
$U_{Overall}$	—	overall heat transfer coefficient, W m ⁻² K ⁻¹
v	—	specific volume, m ³ kg ⁻¹
v_p	—	the pore volume, cm ³ g ⁻¹
X	—	salt concentration, mg L ⁻¹

Subscripts

a	—	adsorbate
ads	—	adsorption
Brine	—	concentrated brine
ch	—	chilled water
Cond	—	condenser
cw	—	cooling water
d	—	distillate
Evap	—	evaporator
g	—	gaseous phase
hw	—	hot water
HX	—	heat exchanger
in	—	inlet

l	—	liquid
des	—	desorption
out	—	outlet
reg	—	regeneration
s	—	salt/adsorbent
sg	—	silica gel
ss	—	stainless steel
v	—	vapour
w	—	wall

References

- <http://www.un.org/waterforlifedecade/background.shtml>
- http://www.2030waterresourcesgroup.com/water_full/
- Jim S. Wallace, Peter J. Gregory, Water resources and their use in food production systems, *Aquatic Science* 64 (2002) 363–375.
- P. Pinstруп-Andersen, R. Pandya-Lorch, M.W. Rosegrant, The World Food Situation: Recent Developments, Emerging Issues, and Long-term Prospects, IFPRI, Washington, DC, 1997.
- V. Frenkel, Desalination methods, technology and economics, in: Desalination Conference, Santa Barbara, CA, April 16, 2004.
- <http://webworld.unesco.org/water/ihp/db/shiklomanov/summary/html/summary.html#5.%20Water>
- Semih Otles., Serkan Otles, Desalination techniques, *Electronic journal of Environmental, Agricultural and Food Chemistry* 4 (2004) 963–969.
- Paul Alois, Global water crisis overview. Available from: <http://www.arlingtoninstitute.org/wbp/global-water-crisis/441#>, 2007.
- GWI DesalData/IDA, 21st GWI/International Desalination Association Worldwide Desalting Plant Inventory, Desalination in 2008, Global Market snapshot (2008).
- Lisa Henthorne, The current state of desalination. Available from: <http://www.idadesal.org/PDF/the%20current%20state%20of%20desalination%20remarks%20nov%2009%20by%20lisa%20henthorne.pdf>.
- M.A. Darwish, N.M. Al-Najem, Energy consumption by multi-stage flash and reverse osmosis desalters, *Applied Thermal Engineering* 20 (2000) 399–416.
- Masahiro Murakami, *Managing Water for Peace in the Middle East: Alternative Strategies*, United Nations University, Tokyo, 1995.
- K.S. Spiegler, Y.M. El-Sayed, *A desalination primer*, Balaban Desalination, Santa Maria Imbaro, 1994.
- O.K. Buros, *The ABCs of desalting*, second ed., International Desalination Association, Topsfield, MA, 2000.
- James E. Miller, Review of Water Resources and Desalination Technologies, <http://prod.sandia.gov/techlib/access-control.cgi/2003/030800.pdf>, 2003.
- John MacHarg., Thomas F. Seacord, Bradley sessions, ADC baseline tests reveal trends in membrane performance, *Desalination & Water Reuse* 18 (2008) 30–39.
- M. A1-Shammiri, M. A1-Dawas, Maximum recovery from seawater reverse osmosis plants in Kuwait, *Desalination* 110 (1997) 37–48.
- Nikolay Voutchkov, Advances in seawater desalination technology, *Water Conditioning & Purification Magazine* 49 (2007) <http://www.wcponline.com/pdf/0709Voutchkov.pdf>.
- Kim Choon Ng., Bidyut Baran Saha, Anutosh Chakraborty, Shigeru Koyama, Adsorption desalination quenches global thirst, *Heat Transfer Engineering* 29 (2008) 845–848.
- X. Wang, K.C. Ng, Experimental investigation of an adsorption desalination plant using low-temperature waste heat, *Applied Thermal Engineering* 25 (2005) 2780–2789.
- K.C. Ng, X.L. Wang, L.Z. Gao, A. Chakraborty, B.B. Saha, S. Koyama, Apparatus and method for desalination, SG Patent application number 200503029-1 (2005) and WO Patent no. 121414A1 (2006).
- K.C. Ng, H.T. Chua, C.Y. Chung, C.H. Loke, T. Kashiwagi, A. Akisawa, B.B. Saha, Experimental investigation of the silica gel–water adsorption isotherm characteristics, *Applied Thermal Engineering* 21 (2001) 1631–1642.
- A. Chakraborty, B.B. Saha, S. Koyama, K.C. Ng, Specific heat capacity of a single component adsorbent-adsorbate system, *Applied Physics Letters* 98 (2011) 221910, doi: 10.1063/1.3592260.
- Chi Tien, *Adsorption calculations and modeling*, Elsevier Science & Technology Books, Boston, 1994.
- B.B. Saha, T. Kashiwagi, Experimental investigation of an advanced adsorption refrigeration cycle, *ASHRAE Transactions* 103 (1997) 50–58.
- Kim Choon Ng, Anutosh Chakraborty, Sai Maung Aye, Wang Xiaolin, New pool boiling data for water with copper-foam metal at sub-atmospheric pressures: Experiments and correlation, *Applied Thermal Engineering* 26 (2006) 1286–1290.
- Kyaw Thu, K.C. Ng, B.B. Saha, A. Chakraborty, Overall of heat transfer analyses of a heat-driven adsorption chiller at assorted regeneration temperatures, in: *International Symposium on Next-generation Air Conditioning and Refrigeration Technology*, Tokyo, Japan, February 17–19, 2010.
- Kyaw Thu, Bidyut Baran Saha, Anutosh Chakraborty, Won Gee Chun, Kim Choon Ng, Study on an advanced adsorption desalination cycle with evaporator–condenser heat recovery circuit, *International Journal of Heat and Mass Transfer* 54 (2011) 43–51.
- K. Thu, K.C. Ng, B.B. Saha, A. Chakraborty, S. Koyama, Operational strategy of adsorption desalination system, *International Journal of Heat and Mass Transfer* 52 (2009) 1811–1816.
- Kim Choon Ng, Kyaw Thu, Hideharu Yanagi, Anutosh Chakraborty, Bidyut B. Saha, Performance analysis of a low temperature waste heat-driven adsorption desalination prototype plant, in: *The 5th Asian Conference on Refrigeration and Air-conditioning*, Tokyo, Japan, June 7–9, 2010.